47th AIAA Aerospace Sciences Meeting and Exhibit, 5–8 January, 2009, Orlando, FL

Proper grid resolutions for the proper basis.

Charles E. Tinney*

Department of Aerospace Engineering and Engineering Mechanics

The University of Texas at Austin, Austin, TX 78712, USA

An investigation into the sensitivity of the convergence of the POD eigenvalues to the discretization of the measurement grid is discussed using a number of different experimental data sets. The purpose is to determine the necessary conditions, base on an *a prior* understanding of the statistical properties of the turbulence field, for sufficiently obtaining a reduced order representation of the flow. The analysis is important for two reasons. The first is that when the grid resolution is too coarse, the eigenvalue energies are underestimated. Conversely, for grid resolutions that are too dense, superfluous information is carried. Where the latter is concerned, the performance of physics based control architectures can be rendered less efficient when inappropriately designed by way of low-dimensional analysis tools.

I. Introduction

Certainly a number of challenges exist when attempting to predict and even control the unsteady behaviors in high Reynolds number turbulent flows. With respect to classical energy cascade models, these flows constitute a broad spectrum of scales ranging from large energy containing structures to small scales which dissipate by means of molecular diffusion. These natural creations have dazzled scientists for centuries; recalling the flow visualizations of Leonardo da Vinci's free water jet.

It is well known that a number of practical systems can be improved by enhancing-, suppressing- or even delaying the transition to- turbulence. However, this is a difficult task considering the spectrum of scales that these flows embody. In light of these obstacles, it is well agreed upon that the large-scale turbulent motions are most important for energy transfer and are indeed well structured events -occurring with varying degrees of predictability. Thus, in order to intelligently control these large flows, robust and reliable predictive methods are required. Given the fidelity of current hardware, these predictive tools are confined to scales on the order of the large coherent structures. Absent of the limitations in current hardware, if other specific features in the flow are more efficient at achieving the desired flow state, then it is important to separate their motions from the various other structures in the flow. In all, physics based structure eduction techniques are resourceful tools for ranking the various events that are a manifestation of the turbulence.

A number of techniques have been proposed for extracting, or separating "large scale" structures from the background turbulence; pseudo flow visualization, conditional sampling, orthogonal decomposition, wavelet transforms. In the current investigation the Proper Orthogonal Decomposition (POD) is used. While the POD does not necessarily select physical structures, it does create a set of functions that have been optimized by way of the turbulent stresses: the fluctuating mechanisms that characterize flows. A growing number of demonstrations of these techniques, as they have been applied to problems concerning turbulent flows, can be found in the literature.[6,12,1,3,14,19,13,9,15,8,18]

Like any other technique, POD requires attention to certain details about the system it is applied in order to ensure accurate representation of the system's low-dimensional features. In this research article an effort is undertaken to produce a generic set of guidelines by which one could estimate the degree to which the POD eigenvalues are over- or under-predicted in their system, given: (a) the density of the measurement

*Assistant Professor, AIAA Senior Member. http://www.ae.utexas.edu/facultysites/tinney/

/ modeling grid and (b) a common statistical flow property. Lumley (1970)[11] postulated that the number of modes required to capture most of the energy is proportional to the spatial extent of the inhomogeneity divided by the integral scale. Subsequently, Glauser & George(1992)[7] observed a difference in the convergence of the POD eigenvalues when a 7 probe array was replaced with a 13 probe array; they asserted that the number of realizations N should be of the order of $1+2\delta/\mathcal{L}_i$; δ and $\mathcal{L}_i$ are the shear layer width and integral length scale, respectively. Tinney, Glauser & Ukeiley(2008)[18] recently compared the solutions obtained from different facilities under a range of Mach numbers and Reynolds number and discovered that the variations in the grid densities used by the various authors were responsible for a significant portion of the discrepancies.

Here, the analysis of Tinney *et al.*(2008)[18] is expanded upon to develop a more comprehensive understanding of this important, and often overlooked, measurement / modeling parameter. The analysis requires an *a priori* calculation of the statistical characteristics of the turbulent fluctuations, particularly, the shear layer width (δ) or the various integral scales of length ($\mathcal{L}_l$) and time ($\mathcal{L}_\tau$). In doing so, a link between the sensitivity of the POD eigenvalues to the density of the measurement grid and common flow properties can be made. The significance is that it necessitates a thoughtful consideration for both the physics that one chooses to preserve, and the degree to which small scale energy becomes superfluous to the overall system. The motive for this is two fold. First, as we are inevitably dealing with a discretized system, a grid density that is too coarse may inappropriately rank the relative energies of the mode constituents. This is more commonly found when experimental techniques are employed as the number of measurement points are typically dictated by either budgetary constraints or physical accessibility to the flow variable (transducer diaphragm or sensing length). Secondly, for grids that are too dense, the excess carryover can hinder the performance of real time estimation and prediction, where closed loop control is concerned. This typically occurs using simulated databases as certain criteria are instituted for stable solution of the governing equations. Since most controller development is performed off-line, *posteriori* corrections for this can be inserted.

The outline of the paper begins with a retracing of Lumley's (1967)[10] classical POD technique in order to establish a basic framework for the sensitivity study. After which, the databases used for the purposes of this study will be described and comprise measurements from two different experiments at two different facilities and of two different flow quantities: near-field velocity and near-field pressure. The motive will be to develop a comprehensive but sensible set of criteria, applicable to a host of other problems in fluid/thermal sciences. Thus, the two databases are chosen specifically in order to provide a more comprehensive understanding of this problem.

II. Proper Orthogonal Decomposition (POD)

Lumley's (1967)[10] Proper Orthogonal Decomposition is well recognized for its capacity to rank the modal constituents within an inhomogeneous and spatially correlated field; details describing the technique can be found elsewhere in the literature.[6,1] The generic form of the technique involves a linear integral equation of the Fredholm type following the Hilbert-Schmidt theory for symmetric integral kernels:

$$\int R_{ij}(x,x')\phi_j^{(n)}(x')\mathrm{d}x' = \lambda^{(n)}\phi_i^{(n)}(x) \tag{1}$$

Here $R_{ij}(x,x')$ is a time averaged cross-correlation tensor constructed from an ensemble of multiple, statistically stationary measurements. The solution to (1) produces an ordered sequence of eigenvalues ($\lambda^{(n)} \geq \lambda^{(n+1)}$) and eigenfunctions that represent more fluctuating energy per mode than any other linear expansion technique. While an infinite number of solutions may exist, they are limited to the resolution of the measured grid. The finite number of eigenfunctions can be used to reconstruct the original instantaneous velocity,

$$u_i(x,t) = \sum_n \mathbf{a}^{(n)}(t)\phi_i^{(n)}(x), \tag{2}$$

using random and uncorrelated expansion coefficients,

$$a^{(n)}(t) = \int u_i(x,t)\phi_i^{(n)*}(x)\mathrm{d}x. \tag{3}$$

whose mean square energies are the eigenvalues themselves: $\lambda^{(n)} = \langle a^{(n)}a^{(q)}\rangle\delta_{(n,q)}$. Typically the convergence of the POD eigenfunctions are shown to display how the energy containing events are ranked and is calculated

from the following energy normalization:

$$\Lambda_{i,o}^{(n)}(x) \;=\; \frac{\lambda_i^{(n)}(x)}{\sum_n \lambda_i^{(n)}(x)}. \tag{4}$$

The denominator in (4) is simply the total cumulative energy and is equal to the total resolved turbulent kinetic energy: $\kappa_i(x)$. Since we are ultimately dealing with a discretized system, the integral in (1) is replaced with a quadrature approximation. The simplest of the quadrature rules are the Riemann sums, (rectangular) whose area under the curve is approximated by a simple rectangle of width dx, and is sufficient for most analyses. Other common approximations include Newton-Cotes formulas, including the trapezoidal and Simpson's rules, and the Gaussian quadrature. The latter of the approximations must be defined independently for all eigenfunctions. Otherwise the weighting function will bias the single mode it was instructed to optimize.

III. Sensitivity Study

A. The near-field velocity of a transonic single stream jet

1. *Experimental description*

Measurements of the velocity field in an axisymmetric transonic jet were acquired by way of stereo Particle Image Velocimetry (PIV). Details of the facility and instrumentation can be found in Tinney *et al.*(2008).[18] The centreline exit velocity U_j of the unheated jet was at a Mach number of 0.85 ($\mathrm{Re}_D = 1 \times 10^6$) and exited from a 50.8mm diameter nozzle into an environment with ambient temperatures around 283°K. The 3-component PIV system was oriented to capture the flow across the (r, θ)-plane of the jet at discrete streamwise locations between $x/D = 3.0$ and 8.0 ($\Delta x/D = 0.25$). An illustration of this configuration is shown in figure 1a.

A total of 1,250 image pairs were acquired at a rate of 4Hz at each streamwise position that the camera and laser sheet optics were traverse to. The characteristic time scale of the flow ($T_t \sim D/U_j = 1.814 \times 10^{-4}$s), indicates that each successive image pair was a statistically independent realization. Image pairs were transformed into vector maps using Dantec Dynamics' FlowManager software (v3.3) with a final cartesian grid density of (y,z)= $(5.0 \times 10^{-2}D, 3.3 \times 10^{-2}D)$. A coordinate transformation y,z,x→ r, θ, x produced radial and azimuthal grid spacings of $\Delta r = 4.17 \times 10^{-2}D$ and $\vartheta = 4°$.

Velocity ratios of the mean (U/U_j) and turbulence (σ_u/U_j) statistics are shown in figure 1b,c using the similarity variable: $\eta = (r - r_{0.5})/x$; x being the downstream distance from the nozzle exit plane while $r_{0.5}$ is the location where the mean velocity is 50% of the jet exit velocity. Additional lines crudely identify the shear layer width δ, found here between $\eta(x) = -0.1$ and 0.17. The definition for δ is sufficient for the purposes of this analysis. The overall collapse of these profiles are consistent with other studies found in the literature.[2,3,9]

2. *The integral eigenvalue problem*

For this data set, the form of the integral eigenvalue problem follows from a number of well documented applications of the POD technique to axisymmetric shear flows[6,3,9,8] and is written here as:

$$\int B_{ij}(r, r', x; m)\phi_j^{(n)}(r', x; m)r'\mathrm{d}r' = \lambda^{(n)}(x; m)\phi_i^{(n)}(r, x; m), \tag{5}$$

where the kernel is constructed from a Fourier-azimuthal transformation of the ensemble averaged two-point velocity correlation:

$$B_{ij}(r, r', x; m) = \frac{1}{2\pi}\int_{-\pi}^{\pi} \langle u_i(r, x, \theta, t)u_j(r', x, \theta + \vartheta, t)\rangle \mathrm{e}^{-i(m\vartheta)}\mathrm{d}\vartheta. \tag{6}$$

The eigenvalues produced from the solution to (5) are normalize by the total resolved energy at each streamwise station in the flow,

$$\Lambda_{i,o}^{(n)}(x) \;=\; \frac{\sum_m \lambda_i^{(n)}(x; m)}{\sum_n \sum_m \lambda_i^{(n)}(x; m)}. \tag{7}$$

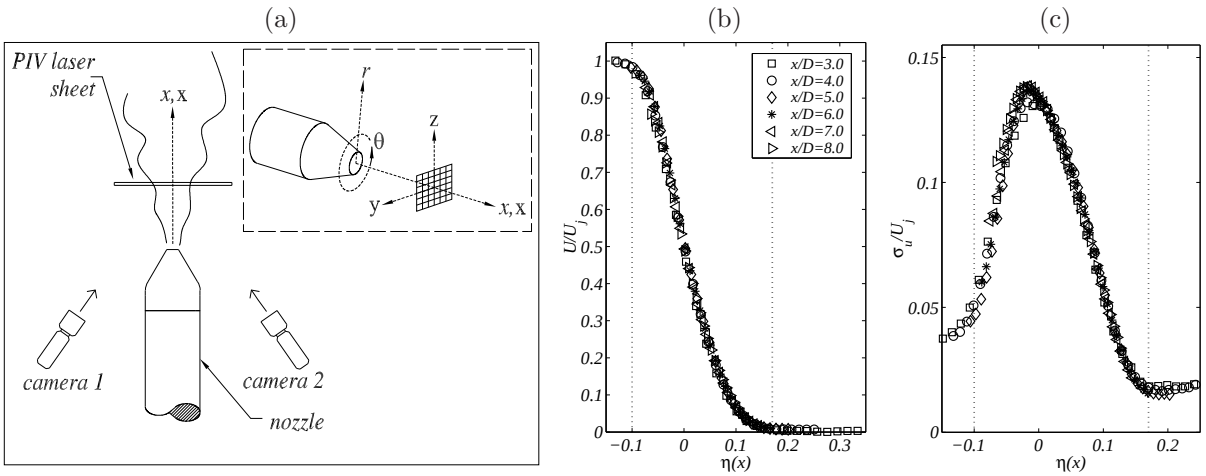

Figure 1. (a) Optical arrangement of the PIV system relative to the transonic jet taken from Tinney, Glauser & Ukeiley (2008b). (b) The mean streamwise velocity, and (c) streamwise turbulence intensities.

A subscript "o" is inserted to segregate between solutions obtained using the original, highly resolved PIV measurement grid and the solutions using grids of varying degrees of coarseness. The variation in the normalized energy of the first five POD modes using the original (highly resolved) grid was found to be within 5% of the averaged normalized values.

3. Transverse integral length scales

Given the nature of these PIV measurements, this analysis is confined to integral lengthscales along the transverse coordinate of the jet (r), defined here as,

$$\mathcal{L}_{l,i}(r,x) = \int_r^{r'} \frac{R_{ii}(r,r',x)}{\sigma_i(r,x)\sigma_i(r',x)} \mathrm{d}r'. \tag{8}$$

These lengthscales are computed for both streamwise and radial components of velocity. In figure 2 (a), the transverse integral lengthscales are extracted from two radial locations in the jet shear layer. The first location identifies where the center of the largest lengthscales are found (towards the low-speed regions of the jet shear layer), while the second location is the value obtained along the lip-line of the jet at $r/D = 0.5$; the differences are subtle. The radial locations where maximum values are obtained is shown in figure 2b. Likewise, ratios between the shear layer width and the integral lengthscale are presented in figure 2c; the shear layer width having been defined earlier as the region between $\eta(x) = -0.1$ and 0.17. At this Mach number, the centerline velocity does not fall below $0.95U_j$ until after $x/D = 6$, and so a subtle decay in $\delta/\mathcal{L}_{l,i}$ around six jet diameters is expected since the jet shear layer's growth is less rapid.

4. Sensitivities

To study the sensitivity of the POD eigenvalues to the discretization of the measurement grid, the original, fully resolved kernel is projected onto a series of grids with increasing coarseness. The projection is performed using a standard triangle-based linear interpolation scheme. Any errors introduced by the interpolation scheme were tracked and found negligible. A sample demonstration of this is shown in figure 5a showing the diagonal (turbulence intensity) of the kernel (streamwise component) at $x/D = 4.0$ after several iterations of interpolation. For this study, the resolution of each interpolated grid (Δr) was scaled by the transverse integral lengthscales, performed over several axial stations in the flow and confined to the shear layer's width. To be certain of the relative differences between the converged solutions and the solutions obtained using the under resolved grids, the following energy normalization was calculated for each POD mode,

$$\epsilon_i^{(n)}(x) \;=\; \frac{\Lambda_i^{(n)}(x) - \Lambda_{i,o}^{(n)}(x)}{\Lambda_{i,o}^{(n)}(x)} \times 100\%. \tag{9}$$

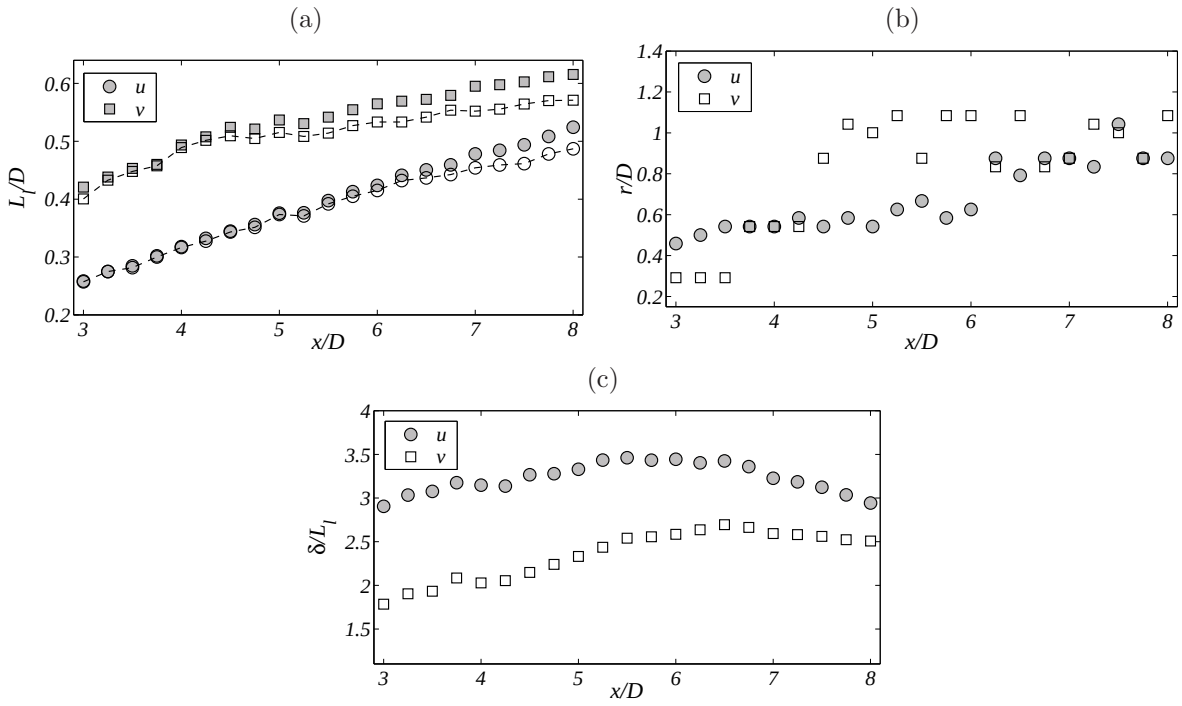

Figure 2. (a) The transverse integral lengthscales of the flow. Closed and open symbols reflect the maximum values and the values obtained along the lip-line ($r/D = 0.5$), respectively. (b) Radial location identifying the location of where the largest transverse integral length scales reside. (c) Ratio between the shear layer width and the transverse integral lengths scales.

The resultant operation is displayed in figure 3 using POD modes $n = 1, 2$ and 6 from the scalar decomposition of the streamwise and radial components of velocity superposed over various axial stations in the flow. The ordinate axes are confined to $\pm 100\%$ error so any trends exceeding these limits were set to $\pm 100\%$. The trends produced by this are clear: the energy in the POD eigenvalues decay asymptotically as the measurement grid becomes finer (as $\Delta r/\mathcal{L}_{l,i} \rightarrow 0$). While it may be unlikely in this particular application for $\Delta r/\mathcal{L}_{l,i}$ to be as high as 1.5 (or greater), the consistency in the trends are supportive of the analysis and of the physical variable chosen, *i.e.* the integral scales of the flow.

These trends present a number of interesting features. Foremost, the first POD eigenvalue converges to within 1% of its expected value when $\Delta r/\mathcal{L}_{l,i}$ <0.3; higher POD modes requiring finer resolution. Furthermore, as POD based norms comprise finite energy, the over prediction of energy in the first POD eigenvalue can adversely effect the energy in higher mode number eigenvalues. Evidence of this is most visible in figure 3c where the sixth POD eigenvalue tends towards gross under predictions in energy as the spatial discretization becomes courser; $\Delta r/\mathcal{L}_{l,i}$ >0.4. This is an important artifact of these discretized systems as an accurate forecast of a reduced-order model may require more than just the first few POD eigenfunctions. The assertion of Glauser & George (1992)[7] that the number of realizations N should be on the order of $1 + 2\delta/\mathcal{L}_{l,i}$ is indeed reflected in these trends.

In an effort to produce a generic roadmap for estimating the level by which the POD eigenvalues are either over or under predicted, the topologies of the eigenvalue sensitivities are displayed for a broader range of POD modes. The motivation is to provide a comprehensive set of criteria that would be applicable to a host of other problems in thermal and fluid sciences. The resulting topologies resulting from the scalar decomposition of the streamwise and radial topologies are displayed in figure 4a,b by simply superposing the trends displayed in figure 3 and confining the contours to a threshold level of $\epsilon_{u,v}^{(n)} = \pm 0.5\%$. An average over all topologies is included. The threshold level unveils three distinct regions: (1) an under predicted region, (2) an over predicted region and (3) a converged region. For a given POD mode number, the threshold value defines the necessary ratio between grid density and integral scale that would ensure accurate convergence of a certain POD mode. If only the first POD mode of the system is required, then a

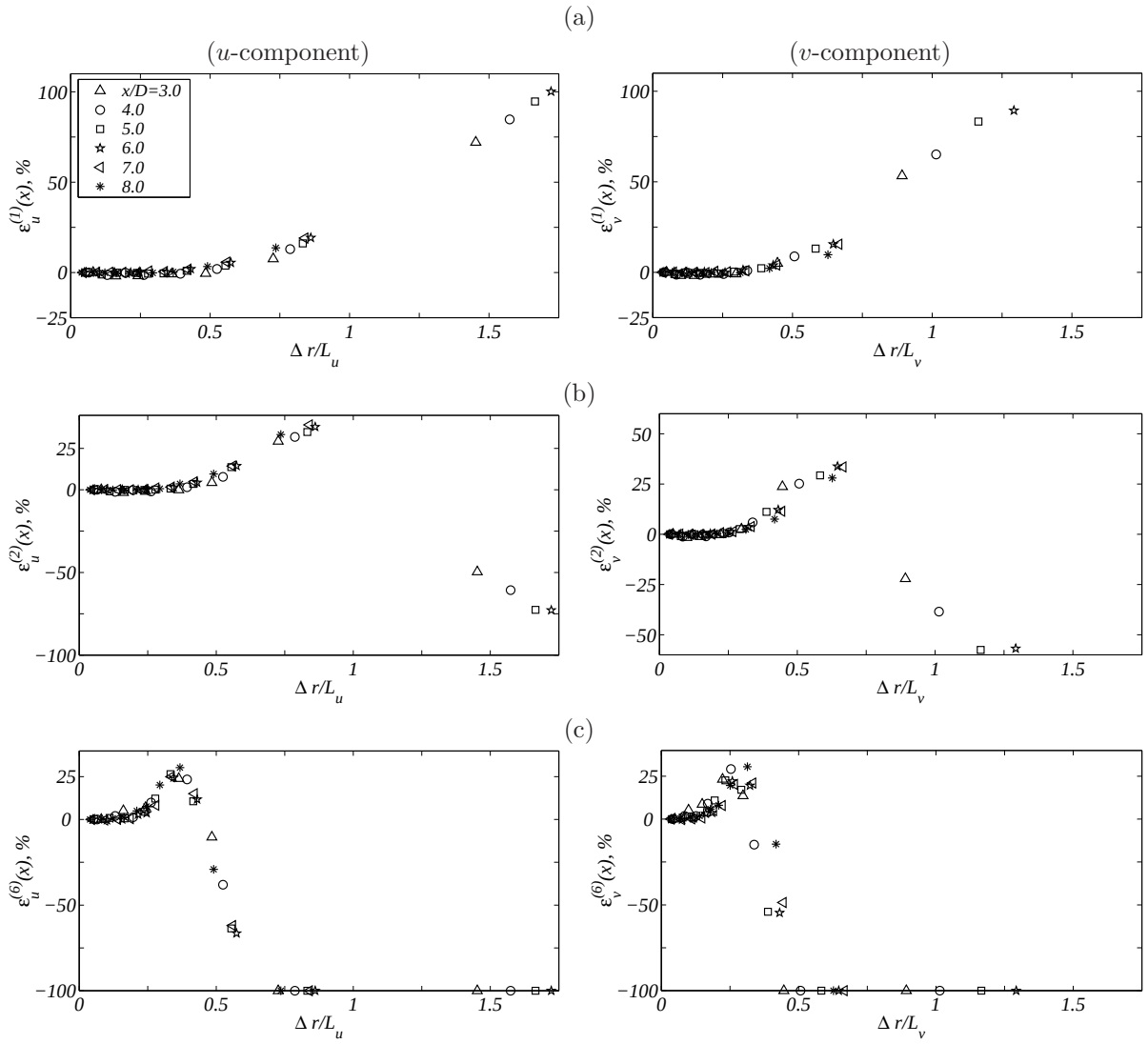

Figure 3. Convergence sensitivity of the POD eigenvalues from the scalar decomposition of the streamwise (left column) and radial (right column) components of velocity. (a) $n = 1$, (b) $n = 2$, (c) $n = 6$.

minimum resolution of $\Delta r/\mathcal{L}_l = 0.3$ is necessary. Thus, with a coarser grid, ($\Delta r/\mathcal{L}_l > 0.3$), the first POD mode's energy is incorrectly predicted, while in a finer grid ($\Delta r/\mathcal{L}_l < 0.3$) superfluous information is carried without significant benefit. A direct comparison of the topologies from the streamwise and radial component sensitivities at the 0.5% threshold is shown in figure 4c; the radial component of velocity appearing to be more sensitive than the streamwise component (demanding greater resolution per mode).

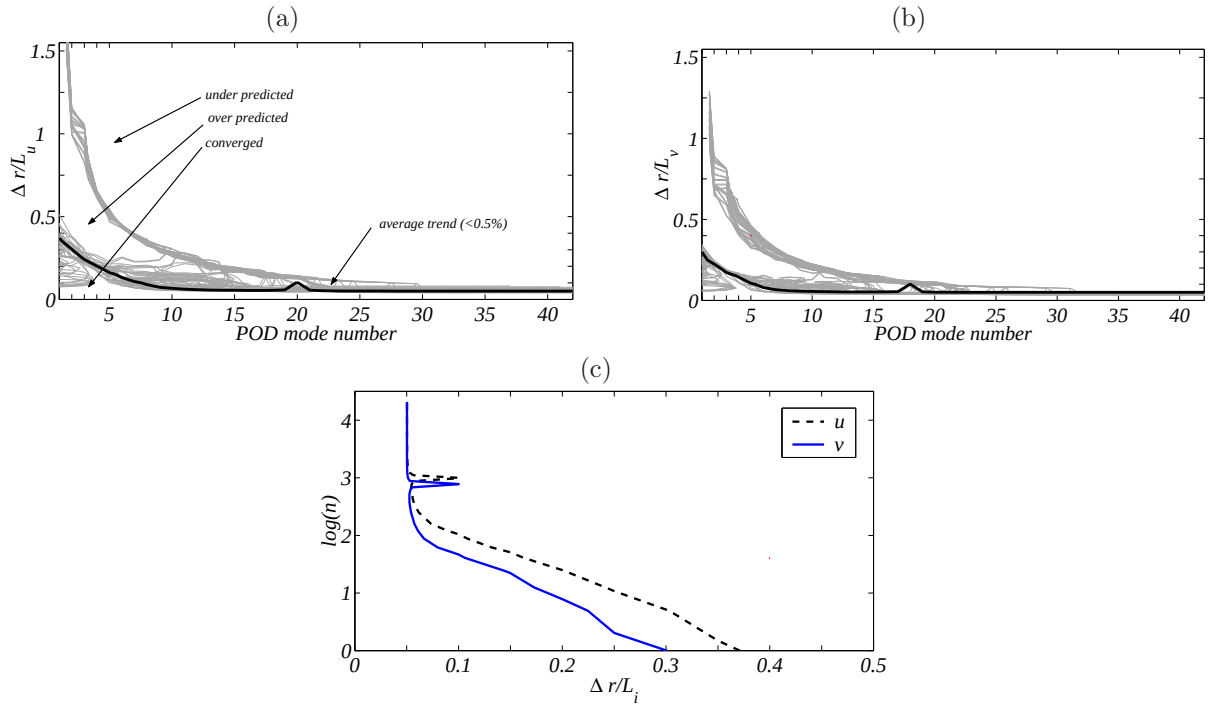

Figure 4. Convergence topology from the scalar decomposition of the (a) streamwise and (b) radial component velocities at a threshold of 0.5%. (c) Comparison of the average threshold at 0.5%

An important question to be addressed at this point is how this behavior should be interpreted physically? An illustrative explanation for this is shown in figure 5a using a sample solution from the streamwise component measurements acquired at $x/D = 4.0$. At this location in the flow, the diagonal of the two-point correlation (the unweighted kernel) is shown after several iterations of interpolation. The first POD eigenfunction (for the zero azimuthal mode) produced during each iteration from the solution to (5) is shown alongside in figure 5b. The out of phase peaks (positive amplitude at $\eta(x) > 0$, negative at $\eta(x) < 0$) in this eigenfunction suggest high-speed (positive) entrainment of fluid into the jet shear layer followed by low-speed (negative) ejections from the potential core. It is correct to assume then that this eigenfunction is spatially out of phase with the jet's fluctuating velocity since it is known that the unsteady ejection of fluid from the potential core occurs at high speeds (positive at $\eta(x) < 0$) while the unsteady entrainment of fluid from the outer regions of the shear layer occurs at low speeds (negative at $\eta(x) > 0$) [a]. Nonetheless, as the measurement / modeling grid becomes finer, the eigenfunction converges to a preferred shape, before which the function peaks at different spatial locations, and is grossly over estimated in amplitude. Such errors, having been introduced because of poor spatial resolution, have falsely represented some features of this flow.

B. The near-field pressure of a transonic coaxial (dual stream) jet.

1. *Experimental description*

In a second phases of this analysis, attention is given to a unique set of measurements taken from an experimental campaign conducted at QinetiQ's Noise Test Facility (NTF) in Farnborough, England as part

[a]The time varying expansion coefficients account for this phase discrepancy and so should be anticipated.

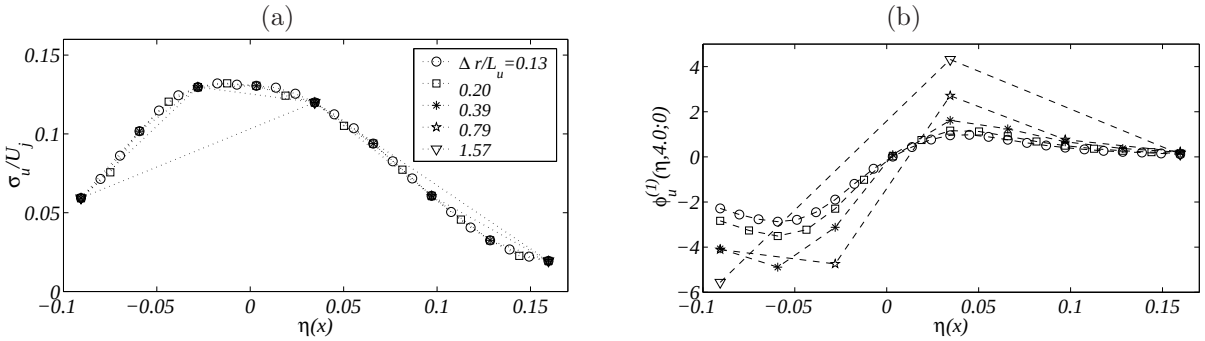

Figure 5. (a) The diagonal of the kernel at $x/D = 4.0$ after several iterations of interpolation. (b) The first POD eigenfunction from the scalar decomposition of the streamwise velocity using various grid densities.

of the EU program CoJeN (AST3-CT-2003-502790). Measurements of this kind comprised a line array of microphones situated in the hydrodynamic periphery of an axisymmetric coaxial jet issuing from a short-cowl nozzle. The nozzle is shown in figure 6a and is representative of current state-of-the-art commercial aircraft propulsion systems. See Tinney & Jordan (2008)[17] for a complete description of the experiment and a discussion of results. The significance of the pressure line array is that it warrants a thoughtful consideration of other turbulent scales that may be of interest (longitudinal space, and time coordinate), or that may otherwise be accessible.

The line array comprised 48 microphones, mounted so as to follow the expanding jet. The first microphone tip was located near the exit plane of the secondary nozzle with an inter-microphone spacing of 50mm. The 1/4inch microphones were sampled at f_s=24096Hz for 5 seconds. Several flow conditions were investigated where the total temperature (T_o) and bypass ratios (U_s/U_p) were varied. However, for simplicity, only one set of conditions will be investigated: $U_s = 307\text{ms}^{-1}$, $U_s/U_p = 0.90$, $T_{so} = 335\text{K}$, and $T_{so}/T_{po} = 0.40$; subscripts p and s denote primary and secondary nozzles/jets, respectively. Based on the exit conditions, the largest time scales of the flow estimated from U_s/D_s, where D_s is 273.4mm, indicates that there were a minimum of 2700 statistically independent samples. Profiles of the axial turbulence intensities are shown in figure 6b to demonstrate the position of the microphone line array relative to the jet flow.

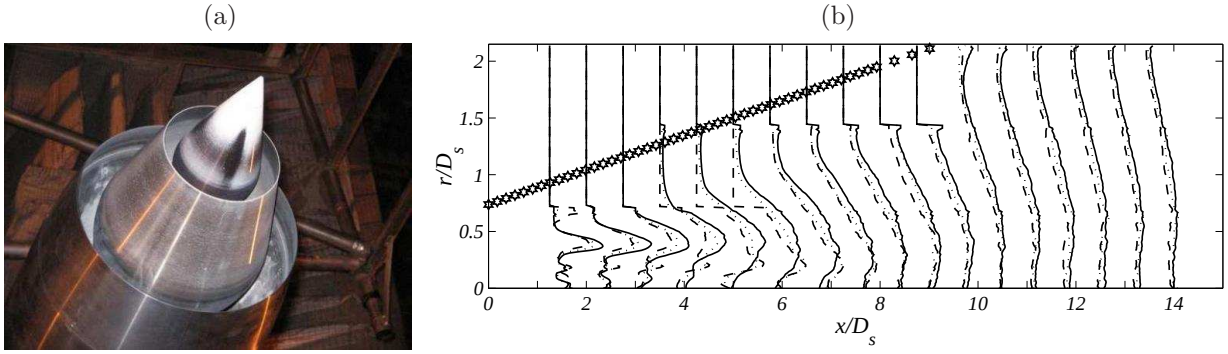

Figure 6. (a) Short-cowl nozzle. (b) Axial turbulence (u'/U_{cl}) velocity ratios of the short cowl nozzle flow for all exit conditions relative to the microphone line array. Taken from Tinney & Jordan (2008a).

2. Longitudinal integral length scales

The mean square values obtained from these measurements are shown in figure 7a with lines identifying regions in the flow where the profile appeared self similar ($x/D_s > 1.27$). That is, structures formed within the first jet diameter are difficult to collapse because they are in a premature state. We are also dealing with measurements acquired within the hydrodynamic periphery of a short-cowl, co-axial nozzle; whilst additional

complications in the near-nozzle region are anticipated. We will discuss the significance of this later on as we address the streamwise similarity of these measurements. For now, we will concern ourselves with the integral length scale ($\mathcal{L}_l$), the integral time scale ($\mathcal{L}_\tau$) and the Taylor microscale ($\mathcal{T}$), calculated here using the following series of definitions:

$$\mathcal{L}_l(x) = \int_X \frac{R_{pp}(x,x')}{\sigma(x)\sigma(x')}\mathrm{d}x', \tag{10}$$

$$\mathcal{L}_\tau(x) = \int_0^\infty |\rho_p(x,\tau)|\mathrm{d}\tau, \tag{11}$$

$$\mathcal{T}(x) = \left[\frac{2\langle p(x,t)^2\rangle}{\langle p_t(x,t)^2\rangle}\right]^{\frac{1}{2}} \tag{12}$$

where $R_{pp}(x,x') = \langle p(x,t)p(x',t)\rangle$, $\rho_p(x,\tau) = \langle p(x,t)p(x,t')\rangle$ and p_t is the time derivative of the pressure: $(\mathrm{d}p/\mathrm{d}t)$. The definition for the Taylor microscale is taken from 6.4.8 of Tennekes & Lumley (1972).[16] These scales are shown in figure 7b; their ratios in figure 7c and d. The convective speed of this flow was determined by Tinney & Jordan (2008)[17] to be approximately $U_c = 0.6(U_s + U_p)/2$ and has been inserted into figure 7d to make it dimensionless. An overall inspection of figure 7 reveals how strongly dependent these integral scales are on the axial location where the correlations are constructed, whilst the difficulty in choosing a sensible criteria for the purposes of this analysis. A plausible correction for this is here discussed.

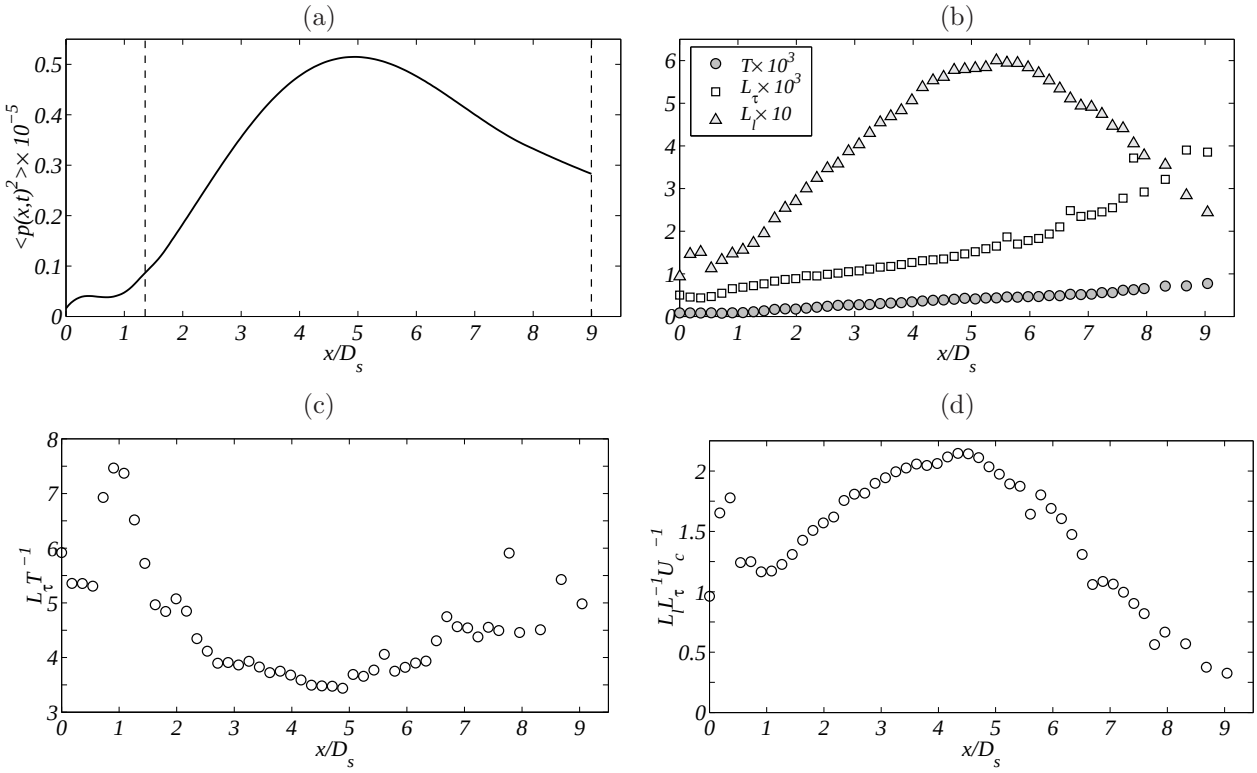

Figure 7. (a) Profile of the mean square pressure. (b) The Taylor microscales ($\mathcal{T}$) and the integral time scales ($\mathcal{L}_\tau$). (c) The ratio of the integral time scale to the Taylor microscale. (d) The ratio of the integral length scale to the integral time scale.

3. Streamwise similarity

Ewing *et al.*(2007)[4] has shown that the solutions for the two-point similarity of the axisymmetric jet depends only on the separation distance between points in the streamwise similarity coordinate. The significance of

the streamwise similarity coordinate is that it rescales the physical coordinate on account of the growth in the turbulent motions as they evolve downstream. The two-point correlation coefficient is given by,

$$\rho_{pp}(\xi,\xi') = \frac{\langle p(\xi,t)p(\xi',t)\rangle}{[p(\xi)^2 p(\xi')^2]^{\frac{1}{2}}}, \tag{13}$$

where $\xi = \ln(x - x_o)$ and x_o is the location of a virtual origin: determined from observation to be around $x/D_s = -0.45$. A good collapse of the two-point correlation coefficient in figure 8a shows how pressure fluctuations of this kind are homogeneous in the streamwise similarity coordinate $(\xi' - \xi)$. This was also shown in Tinney & Jordan (2008).[17] Therefore, by transforming the integral length scale into this coordinate should make this scale homogeneous. In figure 8b the integral length scales $(\mathcal{L}_l)$ are shown for each streamwise similarity position along the array; a mean value of 0.37 has been drawn as a dashed line. Thus, the coordinate transformation produces a viable physical quantity that is independent of coordinates.

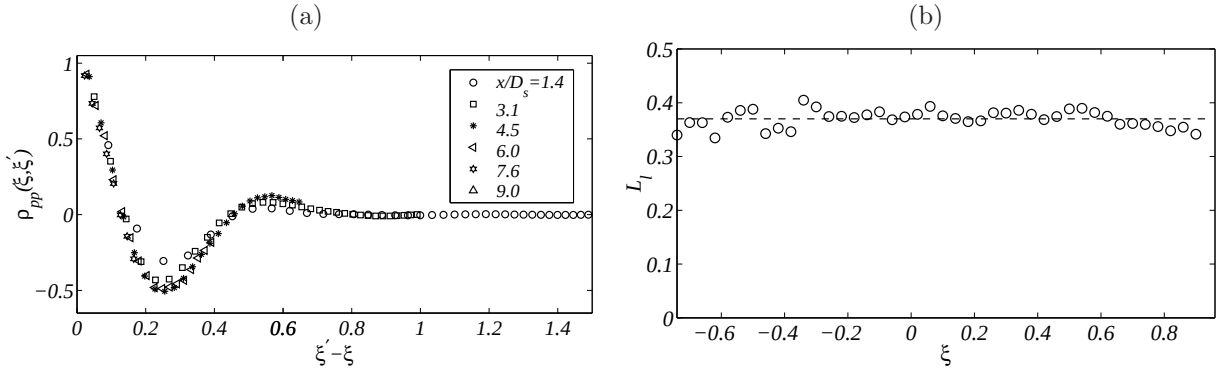

Figure 8. (a) Collapse of the two-point correlation coefficients using the streamwise similarity coordinate. (b) The integral length scale calculated using streamwise similarity coordinates.

4. The integral eigenvalue problem

For this component of the analysis, the sensitivity study is performed by solving the following integral eigenvalue problem:

$$\int R_{pp}(\xi,\xi')\phi_p^{(n)}(\xi')\mathrm{d}\xi' = \lambda_p^{(n)}\phi_p^{(n)}(\xi), \tag{14}$$

using a kernel constructed in streamwise similarity coordinates:

$$R_{pp}(\xi,\xi') = \langle p(\xi,t)p(\xi',t)\rangle. \tag{15}$$

It is the author's understanding that the written form of the integral eigenvalue problem using streamwise similarity coordinates was first proposed by W. K. George.[5] In figure 9, the kernel's topology is plotted in its original coordinate system (9a) alongside its topology in the new transformed streamwise similarity coordinate (9b). Dashed lines in figure 9a identify the domain over which the coordinate transformation and the POD techniques are performed; regions upstream of $x/D_s > 1.27$ have been removed from the analysis due to the complicated near nozzle activity mentioned earlier. In figure 9b the envelop of growth saturation and decay is still present and so the proper basis are expected to retain this feature. The significance of the coordinate transformation is more visible in figure 9c whereby the correlation coefficient is remarkably homogeneous. The solution to (5) produces a set of eigenvalues and eigenfunctions whose features are thoroughly discussed by Tinney & Jordan (2008).[17]

5. Sensitivities

Like the former analysis, the POD eigenvalue's sensitivity to the measurement grid is studied by projecting the kernel (constructed from 15) onto a series of grids with increasing coarseness ($\Delta\xi \to \infty$). The process

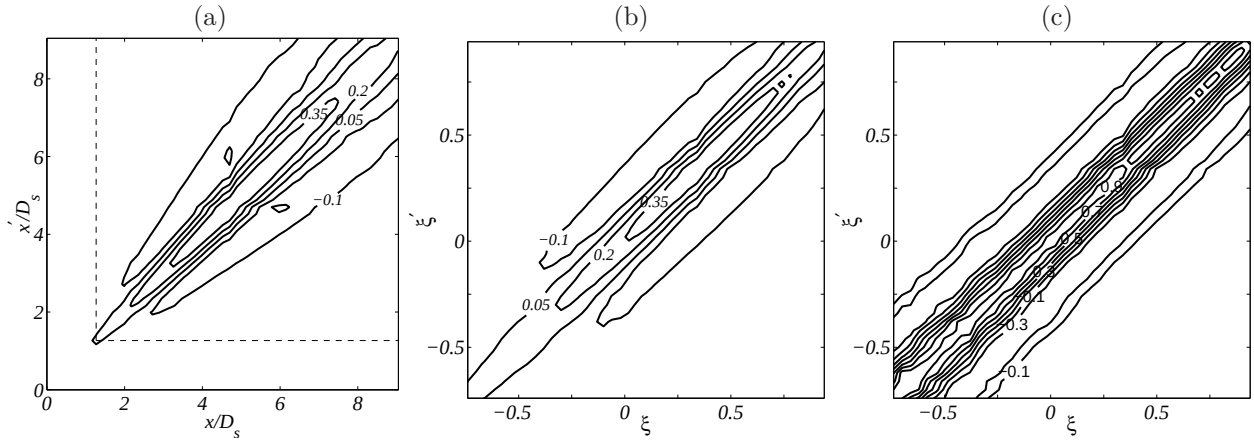

Figure 9. (a) The pressure covariance $R_{pp}(x, x') \times 10^{-5}$ in standard coordinates. (b) The pressure covariance $R_{pp}(\xi, \xi') \times 10^{-5}$ in streamwise similarity coordinates. (c) The pressure two-point correlation coefficient $\rho_{pp}(\xi, \xi')$ in streamwise similarity coordinates.

is performed over several iterations during which the eigenvalues are tracked using the following energy normalization:

$$\epsilon_p^{(n)} = \frac{\Lambda_p^{(n)} - \Lambda_{p,o}^{(n)}}{\Lambda_{p,o}^{(n)}} \times 100\%, \tag{16}$$

where

$$\Lambda_{p,o}^{(n)} = \frac{\lambda_p^{(n)}}{\sum_n \lambda_p^{(n)}}. \tag{17}$$

The resulting operation is shown in figure 10a for the first three POD modes under a range of grid densities between $0.01 < \Delta\xi/\mathcal{L}_l < 1.5$. As $\Delta\xi/\mathcal{L}_l \to \infty$ the energy in the first POD eigenvalue increases substantially, resulting an an under prediction in energy in higher POD modes. Likewise, the under predicted, over predicted and fully converged solutions are manifest in figure 10b using a threshold value of 3%. As we are incapable of average the solutions from this analysis, (unlike the former study what was averaged over 21 axial flow stations), the noise residing around a threshold value of 0.5% was too great to identify a clear trend. Nevertheless, the results are remarkably similar to the findings reported in figure 3 using the transverse integral length scale of the near field velocity and a 3% threshold.

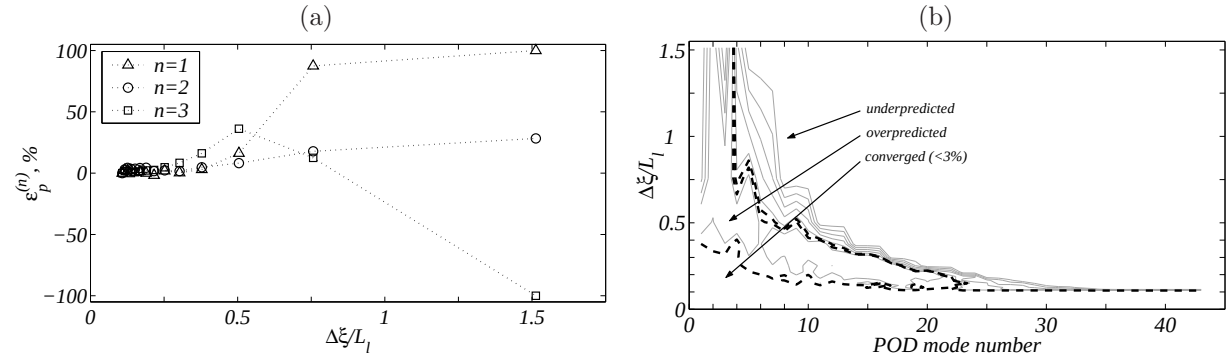

Figure 10. (a) Convergence sensitivity of the first three POD eigenvalues. (b) Convergence threshold at 3%.

IV. Conclusions

By expanding on the analysis of Tinney *et al.*(2008),[18] this study has quantified the degree to which the energy in the POD eigenvalues are dependent on the resolution of the measurement / modeling grid. Previous assertions of Lumley (1970)[11] and Glauser & George (1992)[7] are supported by this analysis. That is, the number of modes required to capture most of the energy is proportional to the spatial extent of the inhomogeneity divided by the integral scale and that the number of realizations should be of the order of $1 + 2\delta/\mathcal{L}_i$, respectively.

Two important concerns are addressed when selecting the proper grid for the proper basis. The first is more commonly found in experimental databases where coarse grids, dictated by either budgetary constraints or physical accessibility to the flow variable, may result in poor predictions in energy of the various mode constituents. In particular, a grid that is too coarse will over predict the energy in the first few POD modes. Likewise, as we are dealing with a system of finite energy, this over prediction trickles to higher POD modes whose energies become under predicted. The second item is more concerning to the numerical community where stable solution of the governing flow equations necessitates high spatial resolutions, often exceeding what is demanded for accurate modeling of a low-order dynamical system. The superfluous information adds no benefit to the stability of the system, and so its performance is potentially hindered.

Furthermore, it is commonly understood that if the convergence of the POD eigenvalues is rapid, the ratio of the energy containing events (the coherent mechanisms) to the background turbulence (incoherent noise) is large. Conversely, if the POD eigenvalues converge lass rapidly, in relation to the former, the ratio is small. Thus the rate by which the eigenvalues converge is a useful indicator of how coherent the system is. While this is true in general, the sensitivity to the discretization of the measurement grid is often over looked and so renders such statements invalid if one is inconsiderate of the proper resolutions for obtaining the proper basis.

References

[1]Berkooz, G., Holmes, P. & Lumley, J. L. 1993 The proper orthogonal decomposition in the analysis of turbulent flows. *Annu. Rev. Fluid Mech.* **25**, 539–75.

[2]Bradshaw, P., Ferriss, D. H. & Johnson, R. F. 1964 Turbulence in the noise-producing region of a circular jet. *J. Fluid Mech.* **19**, pp. 591-624.

[3]Citriniti, J. H. & George, W. K. 2000 Reconstruction of the global velocity field in the axisymmetric mixing layer utilizing the proper orthogonal decomposition. *J. Fluid Mech.* **418**, pp. 137–166.

[4]Ewing, D., Frohnapfel, B., George, W. K., Pedersen, J. M. & Westerweel, J. 2007 Two-point similarity in the round jet. *J. Fluid Mech.* **577** 309–330.

[5]George, W. K. *Summer Workshop on Jet Aeroacoustics.* Summer 2006, University of Poitiers, France.

[6]Glauser, M. N. & George, W. K. 1987 Orthogonal decomposition of the axisymmetric jet mixing layer including azimuthal dependence. *Advances in Turbulence* (ed. G. Comte-Bellot & J. Mathieu), 357–366. Springer-Verlag.

[7]Glauser, M. N. & George, W. K. 1992 Application of multipoint measurements for flow characterization. *Experimental Thermal and Fluid Sciences* **11**, 617–632.

[8]Iqbal, M. O. & Thomas, F. O. 2007 Coherent Structures in a Turbulent jet via a vector implementation of the proper orthogonal decomposition. *J. Fluid Mech.* **571**, 281–326.

[9]Jung, D., Gamard, S. & George, W. K. 2004 Downstream evolution of the most energetic modes in a turbulent axisymmetric jet at high Reynolds number. Part 1. the near-field region. *J. Fluid Mech.* **514**, 173–204.

[10]Lumley, J. L. 1967 The structure of inhomogenous turbulent flows. In *Atmospheric Turbulence and Radio Wave Propagation*, (ed A. M. Yaglom & V. I. Tatarski), pp. 166–178. Moscow: Nauka.

[11]Lumley, J. L. 1970 Stochastic Tools in Turbulence. *Academic*, New York.

[12]Moin, P. & Moser, R. D. 1989 Characteristic eddy decomposition of turbulence in a channel. *J. Fluid Mech.* **200**, 471–509.

[13]Noack, B. R., Afanasiev, K., Morzynski, M. & Thiele, F. 1993 A hierarchy of low-dimensional models for the transient and post-transient cylinder wake. *J. Fluid Mech.* **497**, 335–363.

[14]Rempfer, D. 2000 On low-dimensional Galerkin models for fluid flow. *Theor. Comput. Fluid Dyn.* **14**, 75–88.

[15]Rowley, C. W., Colonius, T. & Murray, R. M. 2004 Model reduction for compressible flows using POD and Galerkin projection. *Physica D. Nonlinear Phenomena* **189**(1-2), 115–129.

[16]Tennekes, H. & Lumley, J. L. 1972 A first course in turbulence. *MIT Press.*

[17]Tinney, C.E. & Jordan, P. 2008 The near pressure field of co-axial subsonic jets. *J. Fluid Mech.* **611**, 175–204.

[18]Tinney, C.E., Glauser, M.M. & Ukeiley, L. 2008 Low-dimensional characteristics of a transonic jet. Part 1: Proper Orthogonal Decomposition. *J. Fluid Mech.* **612**, 107–141.

[19]Ukeiley, L., Cordier, L., Manceau, R., Delville, J., Glauser, M. N. & Bonnet, J. P. 2001 Examination of large scale structures in a turbulent plane mixing layer. Part 2: Dynamical Systems Model. *J. Fluid Mech.* **441**, pp. 67–108.